

An Efficient Approach to Calculate Current Distributions for Electro-Deposition of Chip Interconnections*

F. Santosa[†] M. Vogelius[‡]

Abstract

This Technical Note is motivated by the need to develop efficient and accurate computer modeling of the electro-deposition process commonly used in the fabrication of chip interconnections. A main difficulty owes to the fact that the deposition process is controlled at the bulk (wafer) scale, while the chip features to be produced are microscopic by comparison. Therefore, to accurately model the process computationally, the discretization must be done in such a way that the microstructural behavior is captured. A brute force approach to this would result in extremely large computational problems.

Instead we propose an approach based on a combination of multiscale asymptotics and computations. The asymptotics allows us to first compute the solution in the bulk, having averaged out the microstructures. Secondly, the bulk solution, whose computation does not require a very fine discretization, is corrected by adding terms which may be calculated at the microstructural cell level (independently of the bulk solution). Inherent in the approach is the assumption that the microstructure is locally periodic.

We demonstrate the proposed computational approach for a simple 2-D example in order to assess its accuracy. A rigorous mathematical justification of the approach, which can be accomplished using homogenization theory, is deferred.

1 Introduction

Copper interconnection of chips plays an important role in the semiconductor industry. The preferred process for producing copper interconnections is electro-deposition. An excellent account of this technology is found in Dukovic [6]. For so-called ‘through-mask plating’, masks are placed on top of the substrate to

*This research was partially supported by AFOSR MURI grant to the University of Delaware (FS) and NSF grant DMS-9704575 (MV).

[†]School of Mathematics, University of Minnesota, Minneapolis, MN 55455

[‡]Department of Mathematics, Rutgers University, New Brunswick, NJ 08903

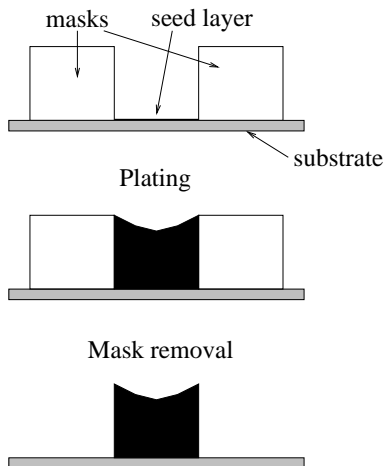


Figure 1: Steps in the through-mask plating.

form ‘trench’-like cross-sections. A seed layer is placed at the bottom of each trench as shown in Figure 1. The ‘masked’ setup is exposed to an electrolyte solution with dissolved copper particles. The electro-chemical process makes the copper particles attracted to the seeded area, so that, after a time, the trenches are filled with copper. The desired interconnect is now obtained by removing the mask.

A chip would typically have hundreds to thousands of interconnects, and the wafer, on which the chips are produced, would contain hundreds of chips. The typical size of interconnects are of the orders of microns, whereas a typical wafer is several inches across. Thus, viewed as single entities, the interconnects are microscopic in comparison to the wafer. A wafer contains tens of thousands of these microscopic features.

The electro-chemical process of electroplating can be modeled by partial differential equations of varying degree of complexity. Given the geometry of the seeded wafer, one can write down the equations that (i) predicts the current density on the seeded regions, and (ii) predicts the shape change of the seeded regions as deposition takes place. Of course these two elements, the current density and the shape change, are coupled [3]. However, in the simplest possible case (when one disregards transport phenomena, and only very crudely models the boundary chemistry) it is very common to use (elliptic) diffusion models to separately characterize the voltage potential (and current flux) and then depend on a simple, explicit relation (e.g. Faraday’s law) to calculate the shape change from knowledge of the normal boundary current density. It is the first step – the computation of the boundary current density, given the seeded wafer geometry – which is the subject of the present work.

Our work exploits the fact that there is a separation of scales in the problem. As noted above, the features of the interconnects are microscopic when

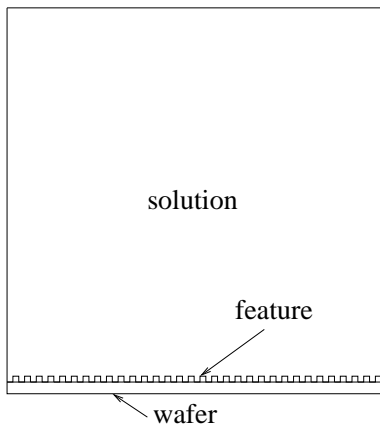


Figure 2: The geometry of fabricating interconnections at the wafer level.

compared to the size of the wafer. This is illustrated in Figure 2. Note that we may also have an intermediate scale, that of ‘patterns’. The approach presented here is sufficiently general that it can be modified to handle all three scales.

In the next section we discuss the idealized model that governs the voltage potential. This is followed by a description of the computational approach we propose. As shall be seen, our approach allows one to effectively deal with situations where the problem cannot be reduced to a single feature-scale problem (with periodic boundary conditions). In section 4, we present results of our numerical computations, and discuss their accuracy. The final section contains some technical details that formally justify our approach.

While only the simplest case of a periodic mask structure is considered, the approach presented here immediately extends to the case where the mask structure is locally periodic. That is, we may consider features that when viewed at a point on the wafer, are periodic, but with a ‘period geometry’ which is allowed to vary as the point of view changes.

2 A model for the electro-plating process

For simplicity we consider a 2-D problem. The ideas of this work extend to 3 dimensions. The electro-plating cell (which contains the electrolytic solution) is represented by the domain

$$\Omega_\epsilon := \{0 < x < 1, \quad \epsilon h\left(\frac{x}{\epsilon}\right) < y < H\} . \quad (1)$$

The small parameter $\epsilon \ll 1$ denotes the feature size. The graph $y = \epsilon h\left(\frac{x}{\epsilon}\right)$ represents the mask structure, the trenches of which are to be filled with copper. The function $h(\cdot)$ is unit periodic. We show a schematic diagram in Figure 3.

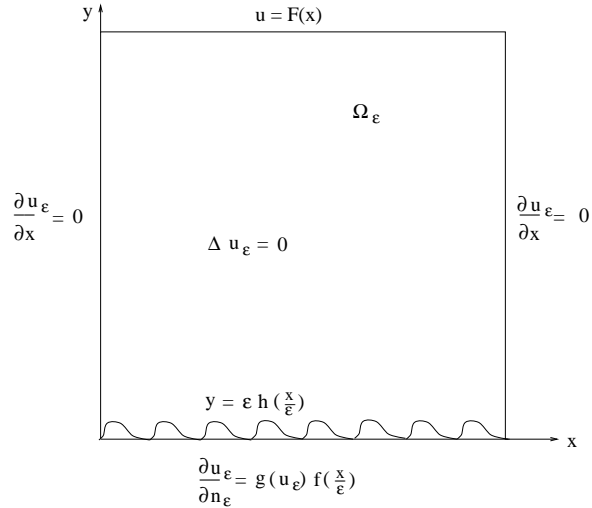


Figure 3: The geometry of the electro-plating problem.

The voltage potential is denoted by $u_\epsilon(x, y)$; the subscript indicates its dependence on the feature scale ϵ . The potential $u_\epsilon(x, y)$ satisfies

$$\Delta u_\epsilon = 0 \quad \text{in } \Omega_\epsilon. \quad (2a)$$

The boundary conditions for $u_\epsilon(x, y)$ are

$$u_\epsilon(x, H) = F(x), \quad \frac{\partial u_\epsilon}{\partial x}(0, y) = \frac{\partial u_\epsilon}{\partial x}(1, y) = 0, \quad (2b)$$

and

$$\frac{\partial u_\epsilon}{\partial n}(x, y) = g(u_\epsilon(x, y)) f\left(\frac{x}{\epsilon}\right) \quad \text{for } y = \epsilon h\left(\frac{x}{\epsilon}\right). \quad (2c)$$

Here the function $f(\cdot)$ is also 1-periodic. The function $f(\cdot)$ allows us to switch back-and-forth between homogeneous Neumann boundary condition and the nonlinear boundary condition represented by the function $g(\cdot)$. We use n for the unit outward normal on the corrugated side. The function $g(\cdot)$ models the appropriate boundary kinetics of the problem. At this point we do not assume anything about the form of g , even though we note that it very frequently is a linear combination of exponentials (the so-called Butler-Volmer model [3]).

The approach proposed here naturally addresses situations where the above problem cannot be reduced to a single periodic problem (unlike those considered in [1]). For example, if the Dirichlet data $F(x)$ in (2b) is not constant, then the problem typically cannot be reduced to a single periodic problem (over a representative period).

Our approach may also be extended to the more general case where the functions $f(\cdot)$ and $h(\cdot)$ are of the form

$$f\left(x, \frac{x}{\epsilon}\right) \quad \text{and} \quad h\left(x, \frac{x}{\epsilon}\right).$$

This would account for the change in the local microstructure with varying x , and would allow us to consider different patterns across a wafer.

The goal is to effectively approximate the flux density $\partial u_\epsilon / \partial n$ along $y = \epsilon h(\frac{x}{\epsilon})$. As described in [6], for the most simple modeling of the shape changes one can then use Faraday's law, stating that the deposition rate is proportional to the current density.

3 A computational procedure for determining current distribution

The basic idea of our computational approach is to separate the phenomena according to scales. It departs from the ansatz that $u_\epsilon(x, y)$ can be written as

$$u_\epsilon(x, y) = u_0(x, y) + \epsilon u_1(x, y, \frac{x}{\epsilon}, \frac{y}{\epsilon}) + O(\epsilon^2). \quad (3)$$

The homogenization based approach (cf. [2, 7, 9]) first solves an 'averaged' equation for the bulk behavior. A detailed microstructural field is then calculated separately and combined with the bulk solution.

The bulk behavior

The function $u_0(x, y)$ is harmonic in the domain without trenches

$$\Delta u_0 = 0 \quad \text{in } \Omega_0. \quad (4a)$$

Ω_0 is the box $\{0 < x < 1, 0 < y < H\}$. This can be viewed as the limit of Ω_ϵ as $\epsilon \rightarrow 0$. The boundary conditions for u_0 are

$$u_0(x, H) = F(x), \quad \frac{\partial u_0}{\partial x}(0, y) = \frac{\partial u_0}{\partial x}(1, y) = 0, \quad (4b)$$

and

$$-\frac{\partial u_0}{\partial y}(x, 0) = g(u_0(x, 0)) \int_0^1 f(\xi) \sqrt{1 + h'(\xi)^2} d\xi. \quad (4c)$$

In the boundary condition (4c), the oscillations in height and the oscillatory property of the original boundary condition (2c) have been 'averaged' out. The averaging manifests itself through the integral on the right-hand side of (4c).

The solution $u_0(x, y)$ represents the bulk behavior. It is (the formal) limit of $u_\epsilon(x, y)$ as $\epsilon \rightarrow 0$. The boundary value problem for u_0 problem, because it is on a regular domain, can be solved accurately using a somewhat coarse mesh. We will need to evaluate $\partial u_0 / \partial y(x, 0)$ and $\partial u_0 / \partial x(x, 0)$ to calculate the desired current density.

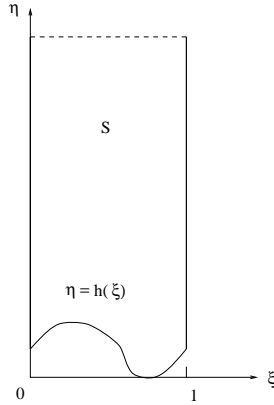


Figure 4: The semi-infinite strip S in the microscopic problem.

The microscopic behavior

The microscopic cell problem we need to solve is linear, even though the boundary condition (2c) is nonlinear. The domain of the problem is the semi-infinite strip given by

$$S = \{(\xi, \eta) : 0 < \xi < 1, h(\xi) < \eta < \infty\} \quad (5)$$

(see Figure 4). The strip is a representative periodic structure viewed in microscopic coordinates. Recall that $h(\xi)$ is unit periodic. We seek functions $v(\xi, \eta)$ and $w(\xi, \eta)$ which satisfy Laplace's equation

$$\Delta v = 0, \quad \Delta w = 0, \quad (6a)$$

are unit periodic, *i.e.*, satisfy

$$\begin{aligned} v(1, \eta) &= v(0, \eta), & w(1, \eta) &= w(0, \eta), \\ \frac{\partial}{\partial \xi} v(1, \eta) &= \frac{\partial}{\partial \xi} v(0, \eta), & \frac{\partial}{\partial \xi} w(1, \eta) &= \frac{\partial}{\partial \xi} w(0, \eta), \end{aligned}$$

and decay as $\eta \rightarrow \infty$

$$v(\xi, \infty) = 0, \quad w(\xi, \infty) = 0. \quad (6b)$$

The boundary condition on the lower part of the boundary is

$$\frac{\partial v}{\partial n}(\xi, h(\xi)) = f(\xi) - \frac{\int_0^1 f(\xi) \sqrt{1 + h'(\xi)^2} d\xi}{\sqrt{1 + h'(\xi)^2}}, \quad (6c)$$

for v , and

$$\frac{\partial w}{\partial n}(\xi, h(\xi)) = -\frac{h'(\xi)}{\sqrt{1 + h'(\xi)^2}}. \quad (6d)$$

for w . In equations (6c)–(6d), n denotes the outward normal to the lower part of the boundary of S . In computing these ‘auxiliary’ functions v and w , we can in practice truncate the domain S at the top, since v and w decay rapidly. Moreover, since this domain is regular (with no microstructure), we can obtain a good approximation to these functions using a fairly coarse mesh.

The bulk corrector

A bulk corrector $U_1(x, y)$ which satisfies Laplace’s equation in the domain Ω_0 is computed. The function $U_1(x, y)$ satisfies homogeneous Dirichlet boundary condition along $y = H$, and homogeneous Neumann conditions along $x = 0$ and $x = 1$. Along the bottom $y = 0$, U_1 satisfies a Robin boundary condition given by

$$\begin{aligned} \partial_y U_1(x, 0) + c_1 g'(u_0(x, 0)) U_1(x, 0) \\ = c_2 \partial_x^2 u_0(x, 0) + c_3 g'(u_0(x, 0)) \partial_x u_0(x, 0) + c_4 g'(u_0(x, 0)) g(u_0(x, 0)) . \end{aligned} \quad (7)$$

The constants c_j , $1 \leq j \leq 4$, are computed from the (already available) microstructural information as follows

$$\begin{aligned} c_1 &= \int_0^1 f(\xi) \sqrt{1 + h'(\xi)^2} d\xi , & c_2 &= \int_0^1 h(\xi) d\xi + \int_0^1 h'(\xi) w(\xi, h(\xi)) d\xi , \\ c_3 &= \int_0^1 h'(\xi) v(\xi, h(\xi)) d\xi - \int_0^1 f(\xi) w(\xi, h(\xi)) \sqrt{1 + h'(\xi)^2} d\xi , \\ c_4 &= \int_0^1 f(\xi) \sqrt{1 + h'(\xi)^2} d\xi \cdot \int_0^1 f(\xi) h(\xi) \sqrt{1 + h'(\xi)^2} d\xi \\ &\quad - \int_0^1 f(\xi) v(\xi, h(\xi)) \sqrt{1 + h'(\xi)^2} d\xi . \end{aligned}$$

The approximate solution and current density

The approximate solution is now obtained by expanding on the ansatz (3). We obtain

$$\begin{aligned} u_\epsilon(x, y) \approx u_0(x, y) + \epsilon \left(g(u_0(x, 0)) v(\xi, \eta) \Big|_{(\xi=\frac{x}{\epsilon}, \eta=\frac{y}{\epsilon})} \right. \\ \left. + \frac{\partial u_0}{\partial x}(x, 0) w(\xi, \eta) \Big|_{(\xi=\frac{x}{\epsilon}, \eta=\frac{y}{\epsilon})} + U_1(x, y) \right) . \end{aligned} \quad (8)$$

The approximate current density at the bottom surface is given by

$$\begin{aligned} \frac{\partial u_\epsilon}{\partial n} \Big|_{y=\epsilon h(\frac{x}{\epsilon})} \approx g(u_0(x, 0)) f\left(\frac{x}{\epsilon}\right) \\ + \epsilon g'(u_0(x, 0)) \left[g(u_0(x, 0)) v\left(\frac{x}{\epsilon}, h\left(\frac{x}{\epsilon}\right)\right) \right. \\ + \partial_x u_0(x, 0) w\left(\frac{x}{\epsilon}, h\left(\frac{x}{\epsilon}\right)\right) + \\ \left. + \partial_y u_0(x, 0) h\left(\frac{x}{\epsilon}\right) + U_1(x, 0) \right] f\left(\frac{x}{\epsilon}\right) . \end{aligned} \quad (9)$$

Note that each quantity on the right-hand side has been calculated, and that each calculation is relatively inexpensive, because we solve for these quantities in regular domains (without any ‘boundary oscillation’). The method presented here can thus be implemented in a computationally efficient manner, as we shall see in the next section.

4 A numerical example

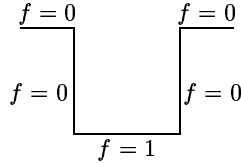
As an illustration of our approach we consider the following problem, whose (nearly) exact solution can also be obtained by a standard finite element package with high accuracy. Let $u_\epsilon(x, y)$ satisfy Laplace’s equation in the domain

$$\Omega_\epsilon = \{0 < x < 1, \quad \epsilon h\left(\frac{x}{\epsilon}\right) < y < 1.5\},$$

(we choose $H = 1.5$) with h given by

$$h(\xi) = \begin{cases} 0.5 & \text{for } 0 < \xi < 0.25 \text{ and } 0.75 < \xi < 1 \\ 0 & \text{for } 0.25 < \xi < 0.75 \end{cases} . \quad (10)$$

We select ϵ so that $1/\epsilon$ is an integer. Notice that the ‘height’ function describing the trenches has vertical jumps, and thus the derivative of h in the various formulae has to be interpreted in a ‘generalized sense’. Concerning $f(\xi)$, we choose it to be zero everywhere except on the bottom of the trenches (see below).



We assume that the Dirichlet condition in (2b) is $F(x) = 1$. Because of the homogeneous Neumann boundary conditions along $x = 0$ and $x = 1$, the symmetry of the microstructural cell, and the integral number of microstructural cells, the solution will be x -periodic of period ϵ . In fact consider the domain

$$\omega_\epsilon = \{0 < x < \epsilon, \quad \epsilon h\left(\frac{x}{\epsilon}\right) < y < 1\},$$

and let γ_ϵ denote the lower boundary of ω_ϵ . The function $u_\epsilon(x, y)$ is simply the x -periodic extension of the harmonic function (in ω_ϵ) with boundary conditions

$$\frac{\partial u_\epsilon}{\partial x}(0, y) = \frac{\partial u_\epsilon}{\partial x}(\epsilon, y) = 0, \quad u_\epsilon(x, 1.5) = 1,$$

and

$$\frac{\partial u_\epsilon}{\partial n} = g(u_\epsilon) f\left(\frac{x}{\epsilon}\right) \quad \text{along } \gamma_\epsilon,$$

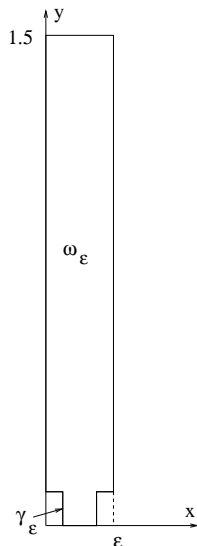


Figure 5: The periodic cell of the boundary value problem. The boundary conditions and the symmetry of each trench allows us to consider the smaller domain. The solution to the boundary value problem is horizontally periodic of period ϵ .

where n denotes the unit outward normal. For our computations we choose $g(z) = \exp(0.2z)$. To obtain a solution to this (and other) two dimensional elliptic boundary value problems we employ Matlab's PDE Toolbox [8]. This package is based on a Finite Element Method using piecewise linear, triangular elements. For the above problem we want a (nearly) exact solution, to be used for comparison with our approximate approach, and with that in mind we base the computations on an adaptively selected mesh with about 7000 triangles (most of the 'mesh refinements' appearing near the upper corners of γ_ϵ). We solve the boundary value problem for $\epsilon = 0.1$ and $\epsilon = 0.2$. The bottom of the trench in each case contains about 20 mesh points. The values of u_ϵ and $\partial u_\epsilon / \partial y$ along this bottom will be used for comparison with those values obtained by our asymptotic/computational approach.

For $h(\xi)$ as given in (10), and $f(\xi)$ as above, we find

$$\int_0^1 f(\xi) \sqrt{1 + h'(\xi)^2} d\xi = 0.5 \quad .$$

The bulk problem (4) with $F(x) = 1$ can be solved explicitly. We use the fact that $u_0(x, y)$ is independent of x in this case. Since $u_0(x, y)$ satisfies Laplace's equation, it is necessarily linear. Thus letting

$$u_0(x, y) = 1 + B(y - 1.5),$$

from the boundary condition at $y = 0$ we obtain

$$-B = 0.5 \exp 0.2(1 - 1.5B).$$

The solution is $B = -0.769217$, giving $u_0 = 2.153826$ and $\partial u_0 / \partial y = -1.538434$ at $y = 0$.

Note that since $u_0(x, y)$ is independent of x , the approximation for the potential (8) and the current density (9) will not involve $w(\xi, \eta)$. As a consequence, for this particular problem we only need to solve the v -problem.

We solve the boundary value problem for $v(\xi, \eta)$ by truncating the region S at $\eta = 10$, and imposing the boundary condition $v(\xi, 10) = 0$. The boundary condition along the lower boundary of S is shown below.

$$\begin{array}{ccc} \frac{\partial v}{\partial \eta} = -0.5 & & \frac{\partial v}{\partial \eta} = -0.5 \\ \frac{\partial v}{\partial \xi} = 0 & & \frac{\partial v}{\partial \xi} = 0 \\ & \frac{\partial v}{\partial \eta} = 0.5 & \end{array}$$

We also use the PDE Toolbox to solve the boundary value problem for $v(\xi, \eta)$.

To obtain the bulk corrector $U_1(x, y)$, we need to evaluate the constants c_j , $j = 1, \dots, 4$, for the Robin boundary condition (7). Since $u_0(x, y)$ is independent of x , we need only calculate c_1 and c_4 . The constant c_1 can be calculated directly from $h(\xi)$ and $f(\xi)$ and is equal to 0.5. To evaluate the constant c_4 we use the just computed values of $v(\xi, \eta)$ along the lower boundary of S . Employing the trapezoidal rule we obtain $c_4 = -0.156267$. The boundary value problem for $U_1(x, y)$ can now be solved explicitly, the solution being

$$U_1(x, y) = -0.096012 y + 0.144018 .$$

In particular, $U_1(x, 0) = 0.144018$.

Now, we may assemble our approximate solution and our approximate current density. We find

$$u_\epsilon(x, y) \approx u_0(x, y) + \epsilon(1.538434 v(\frac{x}{\epsilon}, \frac{y}{\epsilon}) + U_1(x, y)). \quad (11)$$

The approximate current density at the bottom of the trench (the lowest part of γ_ϵ) is given by

$$\begin{aligned} \frac{\partial u_\epsilon}{\partial n} &\approx 1.538434 + \epsilon(0.307687)[1.538434 v + 0.144018] , & (12) \\ &\text{for } 0.25 \leq \frac{x}{\epsilon} \leq 0.75 , \quad y = 0 . \end{aligned}$$

We are ready to assess the accuracy of our approximations. We evaluate the potential approximation (11) along the bottom of the trench at the locations

$\epsilon = 0.1$			$\epsilon = 0.2$		
x	Exact	Approx.	x	Exact	Approx.
0.05000	2.217180	2.216245	0.1000	2.282478	2.278665
0.05625	2.217177	2.216242	0.1125	2.282472	2.278659
0.06250	2.217170	2.216235	0.1250	2.282456	2.278644
0.06875	2.217162	2.216227	0.1375	2.282441	2.278629
0.07500	2.217159	2.216224	0.1500	2.282435	2.278622

Table 1: Comparison of the potential at the trench bottom.

$\epsilon = 0.1$			$\epsilon = 0.2$		
x	Exact	Approx.	x	Exact	Approx.
0.05000	1.558052	1.557640	0.1000	1.578532	1.576845
0.05625	1.558051	1.557639	0.1125	1.578530	1.576844
0.06250	1.558048	1.557637	0.1250	1.578526	1.576839
0.06875	1.558046	1.557634	0.1375	1.578521	1.576834
0.07500	1.558045	1.557633	0.1500	1.578519	1.576832

Table 2: Comparison of the current density at the trench bottom.

indicated in Table 1. Without the order of ϵ correction, the approximate value for the potential is the constant 2.153826. The similar results for the current density approximation (12) at the bottom of the trench are summarized in Table 2. The zeroth order approximation gives a constant current density of 1.538424. The results in Table 1 and 2 indicate that the error of our approximation is relatively small (and of order $O(\epsilon^2)$).

This example only serves to demonstrate the accuracy of our approximation. The strong point, as far as efficiency is concerned, is that this approach can be applied to situations where the original boundary value problem cannot be reduced to a single periodic problem at the microstructural scale. Such a situation arises, for example, (1) if the Dirichlet condition $u_\epsilon(x, H) = F(x)$ is not constant, (2) if the boundary conditions on the sides $x = 0$ and $x = 1$ are not homogeneous, or (3) if the mask structure is only locally periodic (with varying patterns). The approach based on a combination of asymptotics and computations can still be employed to obtain good approximations to the voltages and currents without the need to resort to very fine discretizations.

5 A formal justification of the computational procedure

We start by calculating the normal derivative of u_ϵ along $y = \epsilon h \left(\frac{x}{\epsilon} \right)$

$$\frac{\partial u_\epsilon}{\partial n_\epsilon} = \nabla u_\epsilon \cdot n_\epsilon = \nabla u_\epsilon \cdot \frac{(h', -1)}{\sqrt{1+h'^2}}.$$

Here, n_ϵ denotes the outward normal to the lower boundary of Ω_ϵ . We introduce the ansatz $u_\epsilon = u_0 + \epsilon u_1 + \epsilon^2 u_2 + \dots$, where u_0 depends only on (x, y) , whereas the higher order terms depend on $(x, y, \frac{x}{\epsilon}, \frac{y}{\epsilon})$. (ξ, η) are used to denote the fast variables (x/ϵ and y/ϵ) and it is assumed that the function u_ϵ is 1-periodic in ξ . With this notation

$$\begin{aligned} \frac{\partial u_\epsilon}{\partial n_\epsilon} = & \left(\nabla_{xy} u_0(x, y) + \nabla_{\xi\eta} u_1(x, y, \frac{x}{\epsilon}, \frac{y}{\epsilon}) + \epsilon \nabla_{xy} u_1(x, y, \frac{x}{\epsilon}, \frac{y}{\epsilon}) \right. \\ & \left. + \epsilon \nabla_{\xi\eta} u_2(x, y, \frac{x}{\epsilon}, \frac{y}{\epsilon}) \right) \frac{(h', -1)}{\sqrt{1+h'^2}} + \dots \end{aligned} \quad (13)$$

The $O(1)$ terms in the above right hand side, when evaluated along $y = \epsilon h(\frac{x}{\epsilon})$ give

$$\begin{aligned} & \partial_x u_0(x, 0) \frac{h'}{\sqrt{1+h'^2}} - \partial_y u_0(x, 0) \frac{1}{\sqrt{1+h'^2}} \\ & + \partial_\xi u_1(x, 0, \xi, h(\xi)) \frac{h'}{\sqrt{1+h'^2}} - \partial_\eta u_1(x, 0, \xi, h(\xi)) \frac{1}{\sqrt{1+h'^2}} . \end{aligned}$$

The $O(1)$ term in the right hand side of the boundary condition (2c) is

$$g(u_0(x, 0)) f\left(\frac{x}{\epsilon}\right) . \quad (14)$$

Therefore, equating the $O(1)$ terms from (2c) we get

$$\begin{aligned} & \partial_x u_0(x, 0) h'(\xi) - \partial_y u_0(x, 0) + \partial_{n(\xi\eta)} u_1(x, 0, \xi, h(\xi)) \sqrt{1+h'^2(\xi)} \\ & = g(u_0(x, 0)) f(\xi) \sqrt{1+h'^2(\xi)} . \end{aligned} \quad (15)$$

Let S be the semi-infinite period cell defined by (5). The function $u_1(x, y, \xi, \eta)$ must satisfy

$$\Delta_{\xi\eta} u_1 = 0 \quad \text{in } S ;$$

we naturally require u_1 to be subject to periodic boundary conditions in ξ , and we ask that it has a limit at $\eta = \infty$, that is independent of ξ . The exact value of the limit remains to be determined, however, it is not difficult to see that it will necessarily be attained in a way that

$$\lim_{K \rightarrow \infty} \int_0^1 \frac{\partial}{\partial \eta} u_1(x, y, \xi, K) d\xi = 0 . \quad (16)$$

By integrating the equation $\Delta_{\xi\eta} u_1 = 0$ over $S \cap \{\eta < K\}$, and using (16), we get

$$\begin{aligned} 0 & = \lim_{K \rightarrow \infty} \left(\int_{S \cap \{\eta < K\}} \Delta_{\xi\eta} u_1(x, y, \xi, \eta) d\xi d\eta - \int_0^1 \frac{\partial}{\partial \eta} u_1(x, y, \xi, K) d\xi \right) \\ & = \int_0^1 \partial_{n(\xi\eta)} u_1(x, y, \xi, h(\xi)) \sqrt{1+h'^2(\xi)} d\xi . \end{aligned}$$

Integration of the identity (15) over $0 < \xi < 1$ therefore yields the following boundary condition for u_0

$$-\partial_y u_0(x, 0) = g(u_0(x, 0)) \int_0^1 f(\xi) \sqrt{1 + h'^2(\xi)} d\xi.$$

To find the boundary condition satisfied by u_1 , we simply rearrange (15)

$$\begin{aligned} & \partial_{n(\xi\eta)} u_1(x, 0, \xi, h(\xi)) \\ &= g(u_0(x, 0)) f(\xi) - \partial_x u_0(x, 0) \frac{h'}{\sqrt{1 + h'^2}} + \partial_y u_0(x, 0) \frac{1}{\sqrt{1 + h'^2}}, \end{aligned}$$

or, by insertion of the formula for $\partial_y u_0(x, 0)$

$$\begin{aligned} \partial_{n(\xi\eta)} u_1(x, 0, \xi, h(\xi)) &= g(u_0(x, 0)) \left[f(\xi) - \frac{\int_0^1 f(\xi) \sqrt{1 + h'^2(\xi)} d\xi}{\sqrt{1 + h'^2(\xi)}} \right] \\ &\quad - \partial_x u_0(x, 0) \frac{h'(\xi)}{\sqrt{1 + h'^2(\xi)}}. \end{aligned} \quad (17)$$

Let now $v(\xi, \eta)$ and $w(\xi, \eta)$ be harmonic functions in the cell S , with periodic boundary conditions in ξ , with

$$v(\xi, \infty) = 0 \quad \text{and} \quad w(\xi, \infty) = 0,$$

and with the final boundary conditions on $\eta = h(\xi)$ given by

$$\begin{aligned} \partial_{n(\xi\eta)} v &= f(\xi) - \frac{\int_0^1 f(\xi) \sqrt{1 + h'^2(\xi)} d\xi}{\sqrt{1 + h'^2(\xi)}}, \\ \partial_{n(\xi\eta)} w &= -\frac{h'(\xi)}{\sqrt{1 + h'^2(\xi)}}, \end{aligned}$$

respectively. In terms of the functions $v(\xi, \eta)$ and $w(\xi, \eta)$ we can write

$$u_1(x, y, \xi, \eta) = g(u_0(x, 0)) v(\xi, \eta) + \partial_x u_0(x, 0) w(\xi, \eta) + U_1(x, y). \quad (18)$$

We note that the above decomposition is possible due to the fact that the limit $\lim_{\eta \rightarrow \infty} u_1(x, y, \xi, \eta)$ exists and is independent of ξ ; indeed we see that

$$\lim_{\eta \rightarrow \infty} u_1(x, y, \xi, \eta) = U_1(x, y).$$

Since the first two terms on the right hand side of (18) vanish for $\eta = \infty$ (*i.e.*, in our original coordinates these terms are only present in an ϵ size boundary layer) we conclude that the function U_1 must be harmonic in Ω_0 , and must satisfy $\frac{\partial U_1}{\partial x}(0, y) = \frac{\partial U_1}{\partial x}(1, y) = 0$, and $U_1(x, 1) = 0$. The relevant boundary

condition for U_1 on $y = 0$ remains to be determined. With this in mind, we go back to (13) and expand to $O(\epsilon)$

$$\begin{aligned}
\frac{\partial u_\epsilon}{\partial n_\epsilon}(x, \epsilon h) &= \partial_x u_0(x, 0) \frac{h'}{\sqrt{1+h'^2}} - \partial_y u_0(x, 0) \frac{1}{\sqrt{1+h'^2}} \\
&\quad + \epsilon \partial_x \partial_y u_0(x, 0) \frac{h'h}{\sqrt{1+h'^2}} - \epsilon \partial_y^2 u_0(x, 0) \frac{h}{\sqrt{1+h'^2}} \\
&\quad + \partial_{n(\xi\eta)} u_1(x, 0, \xi, h) + \epsilon h \partial_{n(\xi\eta)} \partial_y u_1(x, 0, \xi, h) \\
&\quad + \epsilon \nabla_{xy} u_1(x, 0, \xi, h) \cdot \frac{(h', -1)}{\sqrt{1+h'^2}} + \epsilon \partial_{n(\xi\eta)} u_2(x, 0, \xi, h) + \dots .
\end{aligned} \tag{19}$$

The expansion to $O(\epsilon)$ of the nonlinear term in the boundary condition (2c) is given by

$$\begin{aligned}
g(u_\epsilon(x, \epsilon h)) f\left(\frac{x}{\epsilon}\right) &= g(u_0(x, \epsilon h) + \epsilon u_1(x, \epsilon h, \xi, h) + \dots) f(\xi) \\
&= g(u_0(x, \epsilon h)) f(\xi) + \epsilon g'(u_0(x, \epsilon h)) u_1(x, \epsilon h, \xi, h) f(\xi) + \dots \\
&= g(u_0(x, 0)) f(\xi) + \epsilon \partial_y u_0(x, 0) h(\xi) g'(u_0(x, 0)) f(\xi) \\
&\quad + \epsilon g'(u_0(x, 0)) u_1(x, 0, \xi, h) f(\xi) + \dots .
\end{aligned} \tag{20}$$

The $O(1)$ terms on the right-hand sides of (19) and (20) balance exactly because of the boundary condition (17) for u_1 . Note also that

$$\partial_{n(\xi\eta)} \partial_y u_1(x, 0, \xi, h) = 0 ,$$

as can be seen from the representation for u_1 in (18). Matching the remaining $O(\epsilon)$ terms from (19) and (20), we arrive at

$$\begin{aligned}
&\nabla_{xy} u_1(x, 0, \xi, h) \cdot \frac{(h', -1)}{\sqrt{1+h'^2}} + \partial_{n(\xi\eta)} u_2(x, 0, \xi, h) \\
&= g'(u_0(x, 0)) u_1(x, 0, \xi, h) f(\xi) + \partial_y u_0(x, 0) h(\xi) g'(u_0(x, 0)) f(\xi) \\
&\quad - \partial_x \partial_y u_0(x, 0) \frac{h'h}{\sqrt{1+h'^2}} + \partial_y^2 u_0(x, 0) \frac{h}{\sqrt{1+h'^2}} .
\end{aligned}$$

If we insert the representation for u_1 (from (18)) into the above identity, and rearrange

$$\begin{aligned}
&\frac{h'}{\sqrt{1+h'^2}} [g'(u_0(x, 0)) \partial_x u_0(x, 0) v(\xi, h) + \partial_x^2 u_0(x, 0) w(\xi, h) + \partial_x U_1(x, 0)] \\
&\quad - \frac{1}{\sqrt{1+h'^2}} \partial_y U_1(x, 0) + \partial_x \partial_y u_0(x, 0) \frac{h'h}{\sqrt{1+h'^2}} - \partial_y^2 u_0(x, 0) \frac{h}{\sqrt{1+h'^2}} \\
&\quad + \partial_{n(\xi\eta)} u_2(x, 0, \xi, h) \\
&= g'(u_0(x, 0)) f(\xi) [g(u_0(x, 0)) v(\xi, h) + \partial_x u_0(x, 0) w(\xi, h) + U_1(x, 0)] \\
&\quad + \partial_y u_0(x, 0) h(\xi) g'(u_0(x, 0)) f(\xi)
\end{aligned}$$

After multiplication by $\sqrt{1+h'(\xi)^2}$ and integration this gives

$$\begin{aligned}
& g'(u_0(x,0))\partial_x u_0(x,0) \int_0^1 h'(\xi)v(\xi,h)d\xi - \partial_y U_1(x,0) \\
& + \partial_x^2 u_0(x,0) \int_0^1 h'(\xi)w(\xi,h)d\xi - \partial_y^2 u_0(x,0) \int_0^1 h(\xi)d\xi \\
& = g'(u_0(x,0))g(u_0(x,0)) \int_0^1 f(\xi)v(\xi,h)\sqrt{1+h'(\xi)^2} d\xi \\
& \quad + \partial_x u_0(x,0)g'(u_0(x,0)) \int_0^1 f(\xi)w(\xi,h)\sqrt{1+h'(\xi)^2} d\xi \\
& \quad + U_1(x,0)g'(u_0(x,0)) \int_0^1 f(\xi)\sqrt{1+h'(\xi)^2} d\xi \\
& \quad + \partial_y u_0(x,0)g'(u_0(x,0)) \int_0^1 f(\xi)h(\xi)\sqrt{1+h'(\xi)^2} d\xi .
\end{aligned}$$

Here we have used that all of the three integrals $\int_0^1 h'(\xi)d\xi$, $\int_0^1 h(\xi)h'(\xi)d\xi$, and $\int_0^1 \partial_{n(\xi\eta)}u_2(x,0,\xi,h)\sqrt{1+h'(\xi)^2} d\xi$ vanish. Upon introduction of constants c_j , $1 \leq j \leq 4$,

$$\begin{aligned}
c_1 &= \int_0^1 f(\xi)\sqrt{1+h'^2}d\xi \quad , \quad c_2 = \int_0^1 h(\xi)d\xi + \int_0^1 h'(\xi)w(\xi,h)d\xi \quad , \\
c_3 &= \int_0^1 h'(\xi)v(\xi,h)d\xi - \int_0^1 f(\xi)w(\xi,h)\sqrt{1+h'(\xi)^2} d\xi \quad , \\
c_4 &= \int_0^1 f(\xi)\sqrt{1+h'(\xi)^2} d\xi \cdot \int_0^1 f(\xi)h(\xi)\sqrt{1+h'(\xi)^2} d\xi \\
& \quad - \int_0^1 f(\xi)v(\xi,h)\sqrt{1+h'(\xi)^2} d\xi \quad .
\end{aligned}$$

we finally obtain the following Robin boundary condition for U_1 (cf. (7))

$$\begin{aligned}
& \partial_y U_1(x,0) + c_1 g'(u_0(x,0))U_1(x,0) \\
& = c_2 \partial_x^2 u_0(x,0) + c_3 g'(u_0(x,0))\partial_x u_0(x,0) + c_4 g'(u_0(x,0))g(u_0(x,0)) \quad .
\end{aligned}$$

We have thus derived a complete set of conditions from which to determine $U_1(x,y)$.

With $u_0(x,y)$, $v(\xi,\eta)$, $w(\xi,\eta)$ and $U_1(x,y)$ available, we can use (18) and (20) to arrive at approximate expressions for the boundary voltage potential and current density whose accuracy are better than $O(\epsilon)$. The approximate expression for the voltage potential is immediately seen to be that given by (8). The approximate expression for the current density becomes

$$\begin{aligned}
\frac{\partial u_\epsilon}{\partial n} \Big|_{y=\epsilon h(\frac{x}{\epsilon})} & \approx g\left(u_0(x,\epsilon h\left(\frac{x}{\epsilon}\right)) + \epsilon u_1(x,\epsilon h\left(\frac{x}{\epsilon}\right))\right) f\left(\frac{x}{\epsilon}\right) \\
& = g\left(u_0(x,\epsilon h\left(\frac{x}{\epsilon}\right)) + \epsilon g(u_0(x,0))v\left(\frac{x}{\epsilon},h\left(\frac{x}{\epsilon}\right)\right)\right)
\end{aligned}$$

$$\begin{aligned}
& +\epsilon\partial_x u_0(x,0)w\left(\frac{x}{\epsilon},h\left(\frac{x}{\epsilon}\right)\right)+\epsilon U_1(x,\epsilon h\left(\frac{x}{\epsilon}\right))f\left(\frac{x}{\epsilon}\right) \\
\approx & g\left(u_0(x,\epsilon h\left(\frac{x}{\epsilon}\right))\right)f\left(\frac{x}{\epsilon}\right) \\
& +\epsilon g'(u_0(x,\epsilon h\left(\frac{x}{\epsilon}\right)))\left[g(u_0(x,0))v\left(\frac{x}{\epsilon},h\left(\frac{x}{\epsilon}\right)\right)\right. \\
& \quad \left.+\partial_x u_0(x,0)w\left(\frac{x}{\epsilon},h\left(\frac{x}{\epsilon}\right)\right)+U_1(x,0)\right]f\left(\frac{x}{\epsilon}\right) \\
\approx & g(u_0(x,0))f\left(\frac{x}{\epsilon}\right)+\epsilon g'(u_0(x,0))\partial_y u_0(x,0)h\left(\frac{x}{\epsilon}\right)f\left(\frac{x}{\epsilon}\right) \\
& +\epsilon g'(u_0(x,0))\left[g(u_0(x,0))v\left(\frac{x}{\epsilon},h\left(\frac{x}{\epsilon}\right)\right)\right. \\
& \quad \left.+\partial_x u_0(x,0)w\left(\frac{x}{\epsilon},h\left(\frac{x}{\epsilon}\right)\right)+U_1(x,0)\right]f\left(\frac{x}{\epsilon}\right) \\
= & g(u_0(x,0))f\left(\frac{x}{\epsilon}\right) \\
& +\epsilon g'(u_0(x,0))\left[g(u_0(x,0))v\left(\frac{x}{\epsilon},h\left(\frac{x}{\epsilon}\right)\right)\right. \\
& \quad \left.+\partial_x u_0(x,0)w\left(\frac{x}{\epsilon},h\left(\frac{x}{\epsilon}\right)\right)+\right. \\
& \quad \left.+\partial_y u_0(x,0)h\left(\frac{x}{\epsilon}\right)+U_1(x,0)\right]f\left(\frac{x}{\epsilon}\right) .
\end{aligned}$$

Note that the last expression is exactly that given by (9).

Remark. If there is no corrugation of the boundary, but only a rapidly varying boundary condition (*i.e.* if h identically equal to zero, but f is not) then the term $\partial_x u_0(x,0)w\left(\frac{x}{\epsilon},h\left(\frac{x}{\epsilon}\right)\right)+\partial_y u_0(x,0)h\left(\frac{x}{\epsilon}\right)$ drops out of the above approximate expression for the flux density, and we end up with

$$\begin{aligned}
\frac{\partial u_\epsilon}{\partial n}\Big|_{y=0} \approx & g(u_0(x,0))f\left(\frac{x}{\epsilon}\right) \\
& +\epsilon g'(u_0(x,0))\left[g(u_0(x,0))v\left(\frac{x}{\epsilon},0\right)+U_1(x,0)\right]f\left(\frac{x}{\epsilon}\right) ,
\end{aligned}$$

with v solving the appropriate elliptic boundary value problem on the “flat” cell $\{0 < \xi < 1, 0 < \eta < 1\}$.

6 Discussion

We have described an approach that allows for the efficient computation of the current density in an electroplating process. The approach exploits the existence of two scales; the scale of the wafer and the scale of the features. It divides the problem into two separate problems by first solving the bulk (averaged) problem, and then next calculating the microstructural detail. The solutions from these two sub-problems are combined to produce an accurate approximation of the electric field. The approach provides quite accurate approximations without the use of extremely large computational meshes.

The approach proposed here is quite general and can be applied to more complicated situations than that described here. An example would be when one has an intermediate scale at the pattern level. The approach can also be modified to take into account more complex models, such as those that describe superfilling [4].

The efficiency of the computational approach also permits us to consider control and optimization problems. That is, we can effectively study the problem of finding the best possible applied voltages in order to achieve certain desirable deposition features [5]. The multiscale approach furthermore allows the imposition of such features at the microstructural scale.

References

- [1] P. Andricacos, C. Uzoh, J. Dukovic, J. Horkans, and H. Deligianni, Damascene copper electroplating for chip interconnections, *IBM Journal of Research and Development*, Vol 42 (1998), pp. 567–574.
- [2] A. Bensoussan, J.L. Lions and G. Papanicolaou, *Asymptotic Analysis of Periodic Structures*, North-Holland, Amsterdam 1980.
- [3] J. Deconinck, *Current Distributions and Electrode shape Changes in Electrochemical Systems*, *Lecture Notes in Engineering*, **75**, Springer-Verlag, Berlin 1992.
- [4] H. Deligianni, J. Dukovic, P. Andricacos, and E. Walton, A model of superfilling in damascene electroplating, preprint 1999.
- [5] H. Deligianni, J. Dukovic, and S. Mehdizadeh, Computational aspects of the terminal effect on wafer-scale uniformity, preprint 1999.
- [6] J. Dukovic, Current distribution and shape change in electrodeposition of thin films for microelectronic fabrication, in *Advances in Electrochemical Science and Engineering*, Volume 3, Gerisher and Tobias, eds., Weinheim, 1994, pp. 117–161.
- [7] A. Friedman and B. Hu, A boundary value problem for the Poisson equation with multiscale oscillating boundary, *J. Diff. Eq.*, **137** (1997), pp. 54–94.
- [8] L. Langemyr, et al., *Partial Differential Equation Toolbox*, Mathworks, 1995.
- [9] F. Santosa, M. Vogelius, and J. Xu, An effective nonlinear boundary condition for a corroding surface. Identification of the damage based on steady state electric data, *Z. Angew. Math. Phys.*, **49** (1998), pp. 656–679.